Diurnal variations of NO_2 tropospheric vertical column density over the Seoul Metropolitan Area from the Geostationary Environment Monitoring Spectrometer (GEMS): seasonal differences and the influence of the *a priori* NO_2 profile

Seunghwan Seo[1], Si-Wan Kim[1,2*], Kyoung-Min Kim[1], Andreas Richter[3], Kezia Lange[3], John P. Burrows[3], Junsung Park[4**], Hyunkee Hong[5], Hanlim Lee[4], Ukkyo Jeong[4], Jung-Hun Woo[6***], and Jhoon Kim[1*]

[1]Department of Atmospheric Sciences, Yonsei University, Seoul, Republic of Korea

[2]Irreversible Climate Change Research Center, Yonsei University, Seoul, Republic of Korea

[3]Institute of Environmental Physics, University of Bremen, Bremen, Germany

[4]Division of Earth Environmental System Science, Major of Spatial Information Engineering, Pukyong National University, Busan, Republic of Korea

[5]National Institute of Environmental Research, Incheon, Republic of Korea

[6]Department of Technology Fusion Engineering, College of Engineering, Konkuk University, Seoul, Republic of Korea

*To whom correspondence should be addressed:

Si-Wan Kim (e-mail: siwan.kim@yonsei.ac.kr) and Jhoon Kim (e-mail: jkim2@yonsei.ac.kr).

[**]now at: Center for Astrophysics | Harvard & Smithsonian, Cambridge, MA, USA

[***]now at: Graduate School of Environmental Studies, Seoul National University, Seoul, Republic of Korea

Date: 10/13/2024

Abstract

The Geostationary Environment Monitoring Spectrometer (GEMS), launched in 2020, provides both temporally and spatially continuous air quality data from geostationary Earth orbit (GEO). This study first investigates the seasonal variations and diurnal behavior of nitrogen dioxide (NO_2) tropospheric vertical column densities (TropVCDs) over the Seoul Metropolitan Area (SMA) using GEMS data, retrieved by the IUP-UB algorithm. We find that the magnitude of the NO_2 TropVCDs and its diurnal behavior have significant seasonal dependences. In January, the highest NO_2 TropVCD values in the range 27.5 – 28.9 × 10^{15} molec. cm^{-2} during the four seasons were observed at 15:00 local time (LT), and NO_2 TropVCD increases from the first retrieved values at 10:00 LT. On the other hand, we find the lowest values (7.4 – 8.8 × 10^{15} molec. cm^{-2}) are at ~14:00 LT in July. The VCD values in July increased up to 10:00 LT, then decreased until 14:00 LT, bu then began to increase again. These different diurnal behaviors of the TropVCDs in the different seasons reflect the differences in photochemical and meteorological conditions as well as the emissions of NOx. Photochemical transformations are typically more rapid in July and slower in January. The absolute values and diurnal behavior of NO_2 TropVCDs are significantly influenced by the wind speed, except in July. Moderate (wind speed ≥ 3m/s) or strong wind (wind speed > 5m/s) reduced the magnitude of the diurnal behavior in January, implying that the NO_2 plumes were transported downwind. Finally, we investigate the retrieved NO_2 TropVCDs with that retrieved using different *a priori* NO_2 data simulated by TM5 and WRF-Chem, calculated using the most recent emission inventories. Although simulated VCDs from WRF-Chem and TM5 show differences of up to a factor 2.75, retrieved NO_2 TropVCDs using each *a priori* data have almost identical values and diurnal behaviors, except in July. Notably, the diurnal behavior of the retrieved NO_2 TropVCDs are independent of those from the two chemical transport models, indicating that observations of slant column densities are the dominant factor in determining the diurnal behavior of NO_2 TropVCDs. Changes of the model horizontal resolution and volatile organic compounds (VOC) emission inventory do not affect significantly the retrieved NO_2 TropVCDs in

this study. However, when the *a priori* NO_2 vertical profile was fixed as the values at 13:45 LT, the diurnal patterns of NO_2 TropVCDs showed significant changes with differences of up to -18.3%.

1. Introduction

Nitrogen dioxide (NO_2) is one of the most important trace gases in the photochemical mechanisms, which determine the tropospheric distributions of ozone and secondary aerosol (Milford et al., 1989). Beginning with the launch of the passive remote sensing instrument GOME om ESA ERS-2 (Burrows et al., 1999) in 1995, then followed by SCIAMACHY on ESA Envisat in 2002 (Burrows et al., 1995 and Bovensmann et al., 1999), OMI on NASA AURA (Levelt et al., 2006), GOME-2 on ESA EUMETSAT Metop A, B and C (Callies et al., 2000, Munro et al., 2016), and TROPOMI on the ESA Sentinel 5 Precursor in 2018 (Veefkind et al., 2012), the amounts and distributions of stratospheric and tropospheric NO_2 vertical column densities (TropVCDs) have been retrieved at increasing spatial resolutions from these instruments, which all fly in sun-synchronous low earth orbit (LEO). By using the retrieved NO_2 TropVCDs from the LEO instruments, the tropospheric nitrogen oxide sources have been identified and their NOx emissions have been estimated, and the chemistry of the troposphere has been studied from the local to the global scale. While instruments on board LEO satellites provide spatially continuous data, observations are obtained only once or twice per day. It was recognized in the late 1990s that instruments similar to SCIAMACHY in geostationary orbit (GEO) would potentially deliver the diurnal variations of key trace gases (see the GeoTROPE concept in Burrows et al., 2004 and references therein). The measurements at the top of the atmosphere of the Geostationary Environment Monitoring Spectrometer (GEMS), launched in 2020, yield the first not only spatially but also temporally continuous air quality data over Asia from the geostationary orbit GEO (see Kim et al., 2020).

Mathematical inversion of the GEMS observations provides diurnal variations of the NO_2 TropVCD. These data products enable the seasonal changes not only in pollutant concentration but also in temporal characteristics, such as the times of the maxima and minima and the sources and sinks of NO_2, which vary by diurnally and seasonally, to be studied for the first time from space.

As part of the differential optical absorption spectroscopy (DOAS) retrieval of NO_2 TropVCD data, air mass factors (AMF) are used to convert slant column density (SCD) to VCD. The assumptions used in the AMF calculation are explained in Richter and Burrows (2002) and Palmer et al (2001). In agreement with other studies, Lorente et al. (2017) reported that the AMF calculation is the largest source of error or uncertainty in NO_2 satellite retrievals. This is because of the assumption used to determine the ancillary or prior data used in the AMF calculation, such as surface albedo, terrain height, cloud parameters, and trace gas profiles. Consequently, the selection of optimal and appropriate *a priori* data is essential to accurately retrieve NO_2 TropVCDs from the observations of any nadir-sounding satellite spectrometer. This is in addition to the need to separate upper atmospheric NO_2 from that in the troposphere.

In this study we investigate two important issues using the GEMS NO_2 TropVCD data over the Seoul Metropolitan Area (SMA): (1) the influence of *a priori* profiles on the retrieved GEMS NO_2 TropVCDs and (2) the seasonal variation of the GEMS NO_2 TropVCD. In section 2 we describe the methods and data used.

Prior to our geophysical interpretation of the NO_2 TropVCD, in Section 3 we compared three GEMS datasets, retrieved with different *a priori* data from the WRF-Chem model. Thereby we investigated the influence of the inventories of the emissions of NOx, defined as the sum of nitrogen monoxide (NO) and nitrogen dioxide (NO_2) in an air mass, on the simulated and retrieved NO_2 TropVCD.

In Section 4, we utilized two chemical transport models (CTM), the Weather Research and Forecast model combined with Chemistry (WRF-Chem) and the global chemistry transport model TM5 (Tracer Model 5) to analyze both the seasonal variations and the influence of *a priori* NO_2 profiles. The seasonal changes in the magnitudes and the time of the maxima of the diurnal NO_2 TropVCD, which we define as the peak times, were investigated. The differences in the spatial distributions of NO_2

TropVCD between the WRF-Chem- and TM5-based GEMS datasets using different *a priori* data, were identified for each season and peak time. We also analyzed the influence of wind speed on the variations in the magnitude and diurnal behavior of the retrieved NO_2 TropVCDs.

2. Data and methods

2.1. GEMS products

GEMS is an ultraviolet-visible (UV-VIS) instrument, measuring contiguously the spectral range from 300 to 500 nm at a spectral resolution of ~ 0.6 nm (Kim et al., 2020). The nominal spatial resolution is 3.5 km × 7.7 km for gases including NO_2 data products. The overall field of regard (FOR) of GEMS covers 75° – 145°E longitude and 5°S – 45°N latitude. GEMS measures hourly during the daytime. The number of observations varies depending on the month, as a result of the length of the day and the measurement strategy. For South Korea, observations are least frequent in January, with six observations per day, and most frequent from April to September, with ten observations per day. We utilized GEMS NO_2 TropVCD data with the IUP-UB algorithm (GEMS IUP-UB products) in January, April, July, and October 2021 – detailed explanations of GEMS IUP-UB products are shown in Section 2.1.1.

2.1.1. GEMS IUP-UB products v1.0

The GEMS NO_2 vertical columns used in this study are from the scientific data product of the University of Bremen, version 1.0 (Lange et al., 2024). NO_2 slant columns are retrieved in the large fitting window 405 – 485nm to reduce noise. In addition to the cross-sections of other absorbing species (O_3, O_4, H_2O and liquid water) pseudo cross-sections for the Ring effect, for GEMS instrument polarization sensitivity and the effects of scene inhomogeneity are included. The stratospheric correction is performed using the STRatospheric Estimation Algorithm from Mainz (STREAM) (Beirle et al., 2016). Conversion to vertical tropospheric columns is based on look-up tables of altitude dependent air mass factors calculated with the radiative transfer model SCIATRAN (Rozanov et al., 2014) using Lambertian equivalent reflectivity (LER) surface reflection values from the TROPOMI climatology (Tilstra et al., 2023). To apply the cloud correction, adjusted cloud fractions and pressure from the GEMS L2 cloud product were used. The NO_2 *a priori* data are different in the different model simulations, which we call runs, as explained below.

2.2. Experiment designs

To analyze the spatiotemporal characteristics of GEMS NO_2 VCDs and the impacts of different *a priori* data on the retrieved values, we undertook five experiments, called TM5, CTRL, CONST, FINE, and MIXED.

The TM5 experiment applies the standard GEMS IUP-UB products v1.0, which use the TM5 model, as their *a priori* data (Huijnen et al., 2010, Williams et al., 2017). The meteorological data for TM5 simulations are obtained from the European Centre for Medium-Range Weather Forecasts (ECMWF) operational forecast data. For the anthropogenic NO_x emission inventory of TM5, the MACCity emission estimates are adopted (Granier et al., 2011), which have no diurnal variation of NO_x emissions. The outputs from TM5 model have a horizontal resolution of 1° × 1° and 34 vertical layers.

For the other four numerical experiments (CTRL, CONST, FINE, and MIXED), WRF-Chem version 4.4 was used to generate *a priori* data (Grell et al., 2005, Skamarock et al., 2021). The chemistry scheme follows the Regional Atmospheric Chemistry Mechanism (RACM) with Secondary Organic Aerosol-Volatility Basis Set (SOA-VBS) option (chem_opt = 108) (Ahmadov et al., 2012). The horizontal resolution of WRF-Chem simulation is 28 km × 28 km, except for the FINE run (12 km × 12 km). All simulations have 59 customized vertical layers. To account for the stratospheric vertical profiles, the Whole Atmosphere Community Climate Model (WACCM) model outputs were combined with the WRF-Chem data (ACOM/NCAR/UCAR, 2020, last access: 05 Dec 2022). The combined data comprises a total of 113 vertical layers. Detailed model configuration is described in Kim et al. (2024). For the anthropogenic emission inventories, the Air Quality in Northeast Asia (AQNEA) emission inventory version 2 was adopted. Since the reference year of AQNEA version 2 is 2019, the anthropogenic NO_x emissions decreased by 20% to account for the decreasing trends of NO_x emissions from 2019 to 2021. We applied the normalized diurnal variabilities of NO_x emissions obtained from the Los Angeles Basin in Kim et al. (2016), but shifting the values one hour earlier (**Figure 1**). For the CONST run, only the *a priori* profiles at 13:45 LT were used to retrieve the NO_2 TropVCD. To investigate the impact on the volatile organic compounds (VOC) emissions of the anthropogenic VOC emissions we used the KORUS emission inventory version 5 (Jang et al., 2020, Woo et al., 2012) in the MIXED run. We retrieved four months (January, April, July, and October 2021) for the TM5 and CTRL runs, and one month (July 2021) for the other runs. The experimental designs are summarized in **Table 1**.

3. Impacts of different *a priori* data on the retrieved NO_2 TropVCDs

We compared retrieved NO_2 TropVCDs from the five different simulations, or runs, to study the impacts of *a priori* data used in AMF calculations on the retrieved NO_2 TropVCD.

3.1. Comparison between the CTRL and TM5 runs

Retrieved NO_2 TropVCDs from the CTRL and TM5 runs exhibit similar diurnal patterns, which are independent of the diurnal patterns of their respective *a priori* data

(**Figure 2**). This suggests that the observed slant column density (SCD) plays a more decisive role in the diurnal pattern of TropVCD than the influence of *a priori* used to determine the AMF. Nevertheless, differences in NO_2 TropVCDs between the two runs were observed, and are particularly noticeable differences in July.

Figure 3 displays spatial distributions of AMF differences between the CTRL and TM5 runs in January, April, July, and October 2021. In urban areas, the AMF in the CTRL run was generally lower (blue) than in the TM5 run, but higher values (red) were observed in the northern and eastern regions of Seoul. As a result, the average values across the SMA domain were similar between CTRL and TM5 – the diurnal patterns of averaged air mass factor over the SMA are shown in **Figure 4**. In July, however, lower values in the CTRL run were observed throughout Seoul and its surrounding areas, leading to lower average AMF values for the SMA region during most of the day. As a result, the TropVCD values in July were higher in the CTRL run (Figure 2c).

In **Figure 5**, we compare NO_2 vertical profiles at 08, 10, 12, 14, and 16 LT from the CTRL and TM5 runs. NO_2 values in the lower atmosphere in the CTRL run are much higher than those in the TM5 run in July, which lead to lower AMF and thus higher NO_2 TropVCD.

3.2. Comparisons between the CTRL and CONST, FINE, and MIXED runs

In **Figure 6**, the diurnal patterns of retrieved and *a priori* NO_2 TropVCDs in July 2021 over the SMA region from the CTRL run and the CONST, FINE, and MIXED runs, are shown. Despite some changes in model resolution and VOC emissions, the FINE and MIXED runs did not show significant differences compared to the CTRL run. In particular, the MIXED run resulted in almost no difference in the *a priori* TropVCD , resulting in nearly identical retrieved NO_2 TropVCD.

On the other hand, the CONST run, which used only the *a priori* vertical profile from 13:45 LT in the retrieval process, exhibited clear differences to the CTRL run. Specifically it had lower values than the CTRL run before ~14:00 LT, but higher values after. These differences are explained by comparisons of vertical profiles from each run, which are displayed in **Figure 7**. The vertical profile shapes of the CTRL, FINE, and MIXED runs are identical, indicating that AMF of each runs have similar values. On the other hand, clear differences of vertical profile shape are apparent between the CTRL and CONST runs. Before 14:00 LT, the CTRL run showed lower sensitivity in the upper layers compared to the CONST run. This indicates a smaller AMF and thus higher VCD values. In contrast, after 14:00 LT, the CTRL run exhibited higher sensitivity to NO_2 in the upper layers of the troposphere, leading to a larger AMF and consequently lower VCD values compared to the CONST run. These differences in the vertical profile arise from effects such as the development of the mixing layer and variations in emissions throughout the day. This implies that providing optimal time-dependent *a priori* data for the AMF calculation will improve the accuracy of the retrieved NO_2 TropVCD.

4. Spatiotemporal characteristics of GEMS NO_2 TropVCD

We report on our investigation of the spatiotemporal characteristics of GEMS NO_2 TropVCD. We use the retrieved NO_2 TropVCD and those simulated by the TM5 and CTRL runs to assess two geophysically important influences on the NO_2 TropVCD the SMA region (126.5 – 127.3°E, 37.2 – 37.8°N) in 2021: (1) the identification, quantification and origin of the seasonal changes; and (2) advection and convection of air masses.

4.1. Seasonal variations

Figure 2 displays diurnal patterns of retrieved and *a priori* NO_2 TropVCDs during weekdays in January, April, July, and October 2021 over the SMA region from the TM5 and CTRL runs. The scenes with wind speed faster than 3m/s are excluded to remove the transport impacts. The effects of transport on NO_2 columns are analyzed in **Section 4.2**.

In January, NO_2 TropVCDs continuously increase from 10:00 local time (LT) to 15:00 LT. During the winter, NO_2 in the urban region accumulates particularly in the boundary layer. Qualitatively, this is explained as follows.

As tropospheric solar UV radiation is low in winter and the atmosphere is cold, photolysis frequencies are small. Similarly, the rate coefficients of many reactions are smaller at the lower winter temperatures compared to those of the other seasons. In winter, the relatively slow loss of NOx occurs through the three body reaction of hydroxyl (OH) with NO_2 to form nitric acid (HNO_3):

$$OH + NO_2 + M \rightarrow HNO_3 + M. \quad (1)$$

The smaller photolysis frequencies of reactions following photoexcitation in the reactions:

$$NO_2 + hv(\lambda < 405\ nm) \rightarrow NO + O \quad (2)$$

$$O_3 + hv(\lambda < 405\ nm) \rightarrow O(^1D) + O_2 \quad (3)$$

lead to slower production of i) the first excited state of oxygen ($O(^1D)$) from the photolysis of ozone (O_3), ii) the hydroxyl radical (OH), and iii) the production of organic peroxyl radicals (RO_2), and hydroperoxyl (HO_2) through the oxidation of methane (CH_4) and VOC. Some of the following reactions are involved:

$$O + O_2 + M \rightarrow O_3 + M \quad (4)$$

$$O(^1D) + N_2 \rightarrow O + N_2 \quad (5)$$

$$O(^1D) + O_2 \rightarrow O + O_2 \quad (6)$$

$$O(^1D) + H_2O \rightarrow OH + OH \quad (7)$$

$$OH + CH_4 \rightarrow CH_3 + H_2O \quad (8)$$

$$CH_3 + O_2 + M \rightarrow CH_3O_2 + M \quad (9)$$

$$CH_3O_2 + NO \rightarrow CH_3O + NO_2 \quad (10)$$

$$CH_3O + O_2 \rightarrow HO_2 + HCHO \quad (11)$$

$$OH + VOC + O_2 \rightarrow nHO_2 + \text{aldehydes} \quad (12)$$

$$OH + CO + O_2 \rightarrow HO_2 + CO_2 \quad (13)$$

$$HO_2 + NO \rightarrow OH + NO_2 \quad (14)$$

Overall at low solar insolation, the low levels of actinic radiation result in smaller amounts of OH and HO_2. The oxidation process is slow and HO_2 and OH chemistry are coupled with NOx chemistry and controlled by rate of oxidation of VOC and CH_4 and the rate of HO_2 to OH through the rate of reaction (14) and the rate of loss of HOx and NOx for example through reaction (1).

In January the maximum values of retrieved TropVCDs are 27.5×10^{15} molec. cm^{-2} (TM5) and 28.9×10^{15} molec. cm^{-2} (CTRL) at 15:00 LT, whereas the *a priori* NO_2 TropVCDs have maxima of 11.2×10^{15} molec. cm^{-2} (TM5) and 21.9×10^{15} molec. cm^{-2} (CTRL) at the same time. These higher values of retrieved NO_2 TropVCDs relative to the model NO_2 TropVCDs are explained by the following inadequate knowledge of the bottom-up diurnal NO_x emissions in January and/or the dilution during the transport of plumes, which is dependent on the model horizontal resolution.

For other months, the maxima of NO_2 TropVCDs occur at earlier times of the day in April at 12:00 LT, in July at 10:00 LT and in October at 11:00 LT. There is also a second maximum at 15:00 LT in October. The behavior of NO_2 TropVCD in April, July and October, when compared to that in January, is explained by the following effects: i) faster tropospheric photolysis frequencies, as a result of higher levels of tropospheric solar insolation and actinic radiation accelerating the photochemical oxidation of CH_4 and VOC in April, July and October compared to January; ii) generally faster reaction rate coefficients of the free radical reactions at the higher temperatures, the rate coefficient of reaction (4) being an exception; iii) the different diurnal emissions of NOx compared to those in January. **Figure 8** shows the diurnal variations of OH concentrations averaged across boundary layer height in each month, calculated by the CTRL model run. The OH concentration in January is about an order of magnitude smaller than that in July.

In April, NO_2 TropVCDs increased until 12:00 LT. It then maintains similar levels until 17:00 LT. The maximum NO_2 TropVCD occurred at 12:00 LT for the CTRL run (21.4×10^{15} molec. cm^{-2}). The maximum NO_2 TropVCD for the TM5 run appeared at 17:00 LT, being 21.9×10^{15} molec. cm^{-2}. However, the retrieved NO_2 TropVCDs from the TM5 and CTRL runs have almost identical behavior up to 15:00 LT. There is a difference of 1.6×10^{15} molec. cm^{-2} (8.1%) between the two runs at 17:00 LT, when *a priori* NO_2 TropVCD value sharply increased from the CTRL run.

In July, both the TM5 (12.2×10^{15} molec. cm^{-2}) and CTRL (13.9×10^{15} molec. cm^{-2}) runs show maxima at 10:00 LT, i.e. the earliest for the four months investigated. After the peak, NO_2 TropVCDs decrease, most likely due to more rapid photochemical loss processes e.g. reaction (1) until 14:00 LT, and then increase. In other seasons, the minimum values were observed in the morning. However, in July, the minimum occurred at 14:00 LT. This unique pattern of behavior is explained by the more rapid photochemical production and removal reactions in summer. We infer that the chemical removal becomes relatively more rapid than the emission and production of NO_2 (see Figure 8). The two types of run show similar diurnal behavior, but the retrieved NO_2 TropVCD of the CTRL runs between 10:00 and 14:00 LT rise to 2.1×10^{15} molec. cm^{-2} i.e. higher than those of the TM5 runs. The diurnal change of *a priori* NO_2 TropVCDs from the CTRL runs shows a similar behavior to that of the retrieved NO_2 TropVCDs, despite the magnitude of *a priori* NO_2 TropVCD being $3.9 – 8.2 \times 10^{15}$ molec. cm^{-2} higher than those retrieved. On the other hand, the *a priori* NO_2 TropVCD from the TM5 runs decreases between 08:00 and 14:00 LT, reflecting diurnally varying photochemistry with similar levels of NO_x emissions throughout the day.

In October, there are broad maxima of NO_2 TropVCD between 12:00 LT and 15:00 LT. Overall diurnal behavior comprises increase up to 12:00 LT, followed by broad maxima, after which the NO_2 TropVCD are similar to those in April.

The highest retrieved values are in the range 25.1×10^{15} to 25.5×10^{15} molec. cm^{-2} for both the TM5 and CTRL runs. As expected, the NO_2 TropVCD are the highest in January and lowest in July.

Figures 9 and **10** show the spatial distributions of retrieved NO_2 TropVCDs in January, April, July, and October 2021 from the TM5 and CTRL runs, respectively. In January, a plume over the SMA region developed as a function of time. Consequently, the suburban areas, which surround the SMA region, experience relatively high NO_2 TropVCD (> 10×10^{15} molec. cm^{-2}) compared to that retrieved in the other months. In April and October, the plumes over the SMA are saturated prior to 12:00 LT and then decrease. In contrast, the NO_2 TropVCD of the surrounding regions are relatively constant or even increase. In July, the overall low values cover the SMA and nearby regions for whole days. The maximum values appear at 10 LT, and then decreased until 14 LT. However, the NO_2 VCD rebounded at 16 LT. **Figure 11** displays the differences between the TM5 and CTRL runs – red color indicates the CTRL run has higher values than the TM5 run; blue means opposite. The CTRL run shows higher VCD values than the TM5 run for all times in July. The largest differences over the SMA region are found at 12 LT in July with differences of 2.1 × 10^{15} molec. cm^{-2}. In other months, the CTRL run generally have higher values of VCD than the TM5 run over the Seoul and urban regions, while there are lower values of VCD from the CTRL run over rural regions.

4.2. Impacts of horizontal transport

Figure 12 shows the diurnal behavior of the retrieved NO_2 TropVCDs from the CTRL run for different wind conditions. The black lines indicate calm runs (wind speed lower than 3m/s), the green line is a strong-wind run (wind speed faster than 5m/s), and the blue lines are the average values with no wind filters. In January (Figure 12a), the diurnal behavior of the NO_2 TropVCDs change significantly with the wind conditions. In the calm run (black solid), NO_2 TropVCD steadily increases due to a combination of the emissions increasing and the slow chemical loss in this month. In windy runs, however, diurnal changes in the retrieved NO_2 TropVCD are negligible.

Although the chemical loss is slow during wintertime, the accumulation of NO_2 was mitigated as strong winds transported large concentrations of NO_2 to downwind regions. The differences between calm and other runs were most significant at 15:00 LT, further indicating that continuous outflow due to transport suppressed the accumulation. As the wind speed increased, there was a noticeable reduction in NO_2 TropVCD values, which indicates a clear inverse relationship between wind speed and VCDs, as shown in Edwards et al. (2024). The values of calm, average (blue solid), and strong wind (green solid) are 19.0 – 28.9, 17.2 – 19.8, and 12.1 – 13.4 × 10^{15} molec. cm^{-2}, respectively.

In April (Figure 12b) and October (Figure 12d), the averaged values with no wind filters (blue solid) have different diurnal behavior, but the maximum NO_2 TropVCD appear almost simultaneously with that of the calm low wind speed run. In

July (Figure 7c), however, the diurnal behavior from the calm run and no wind filters are nearly identical, implying that the wind speeds are overall slow in July.

In summary, the transport effect is maximized in wintertime, changing not only the absolute values but also diurnal behavior of NO_2 Trop VCDs. Consequently, transport must be taken into account when analyzing NO_2 TropVCDs and when estimating top-down NO_x emissions. The role of transport needs to be taken into account even for cases, where the wind speed is relatively slow during summertime (Yang et al., 2024).

5. Conclusions

In this study, we analyzed the seasonal variations and diurnal behavior of the retrieved GEMS IUP-UB NO_2 TropVCD, using the monthly mean data in January, April, July and October. The effects of wind speed, and the impact of *a priori* NO_2 profiles on the retrieval. Both in the CTRL and TM5 runs, the GEMS NO_2 product showed significant changes in quantity, diurnal pattern, and peak time as the seasons changed. In winter, the values were the highest, with a gradual increase over time, whereas in summer, the values were the lowest, reaching a minimum in the afternoon. This is consistent with previous studies, which have shown that atmospheric chemical reactions are more active in summer. Furthermore, we confirmed that wind-driven transport significantly influences the diurnal patterns, clearly demonstrating that advection and possibly convection need to be taken into account when top-down NOx emissions are estimated from an urban agglomeration such as SMA.

On the other hand, when using different *a priori* data to calculate VCD values, more complex results emerged. A comparison between the CTRL and TM5 runs revealed that, despite different spatial resolution and emission characteristics, the retrieved NO_2 TropVCDs exhibited similar diurnal patterns, with significant differences only in July. Additionally, we found that the retrieved NO_2 TropVCDs had diurnal behaviors independent of the *a priori* data in both runs. We infer that the observed SCD has a stronger influence on the retrieved diurnal patterns than *a priori* profiles. Adjusting the horizontal resolution of the model (FINE run) or changing the VOC emissions data (MIXED run) also resulted in no significant differences. However, in the CONST run, where only the vertical profile at 14:00 LT was used in the retrieval process throughout the day, there were significant differences in both the NO_2 Trop VCD values and diurnal patterns. This reaffirms that the vertical shape factor of *a priori* data plays a critical role in NO_2 TropVCD retrievals.

Additionally, given that vertical as well as horizontal model resolution can influence retrievals (Liu et al., 2020), future studies should analyze the results when the vertical resolution is adjusted. Furthermore, as highlighted by previous studies, such as Lorente et al. (2017) and Hong et al. (2017), which emphasized the importance of cloud parameters, aerosol characteristics, and surface albedo, uncertainties arising from factors in addition to the *a priori* NO_2 profile should further be investigated in the retrieval of NO_2 TropVCD for both diurnal GEO observation and those from LEO.

Data availability

GEMS measurement data retrieved by the IUP algorithm are available on request from Andreas Richter (richter@iup.physik.uni-bremen.de). WRF-Chem v4.4 is available in GitHub (wrf-model, 2022).

Author contributions

SWK initiated this study and secured funding. SS and SWK analyzed the satellite and model data. SS, KMK, and SWK conducted the model simulations. AR, KL, and JPB provided GEMS IUP products and analyzed the data. JK, JP, HH, HL, UJ retrieved and analyzed the GEMS observations and discussed the results. JHW provided AQNEA version 2 emission inventory. SS and SWK wrote the paper, with contributions from all co-authors.

Competing interests

At least one of the authors is a member of the editorial board of Atmospheric Measurement Techniques.

Acknowledgement

This work was supported by the National Research Foundation of Korea (NRF) grant funded by the Korea government (MSIT) (No. 2020R1A2C2014131). All the computing resources are provided by National Center for Meteorological Supercomputer. Th contributions from the University of Bremen were supported by the State and University of Bremen and the DLR.

References

Ahmadov, R., McKeen, S. A., Robinson, A. L., Bahreini, R., Middlebrook, A. M., de Gouw, J. A., Meagher, J., Hsie, E.-Y., Edgerton, E., Shaw, S., and Trainer, M.: A volatility basis set model for summertime secondary organic aerosols over the eastern United States in 2006, *J. Geophys. Res. Atmos.*, 117, D06301, https://doi.org/10.1029/2011JD016831, 2012.

Atmospheric Chemistry Observations & Modeling/National Center for Atmospheric Research/University Corporation for Atmospheric Research: Whole Atmosphere Community Climate Model (WACCM) Model Output, Research Data Archive at the National Center for Atmospheric Research, Computational and Information System

Laboratory, https://doi.org/10.5065/G643-Z138, (last access: 05 December 2022), 2020.

Beirle, S., Hörmann, C., Jöckel, P., Liu, S., Penning De Vries, M., Pozzer, A., Sihler, H., Valks, P. and Wagner, T.: The STRatospheric Estimation Algorithm from Mainz (STREAM): Estimating stratospheric NO2 from nadir-viewing satellites by weighted convolution, Atmos. Meas. Tech., 9(7), 2753–2779, doi:10.5194/amt-9-2753-2016, 2016.

Bovensmann, H., Burrows, J. P., Buchwitz, M., Frerick, J., Noël, S., Rozanov, V. V., Chance, K. V., and Goded, A. P. H.: SCIAMACHY: Mission Objectives and Measurement Modes, *J. Atmos. Sci.*, 56, 127-150, https://doi.org/10.1175/1520-0469(1999)056<0127:SMOAMM>2.0.CO;2, 1999.

Burrows J. P., Hölzle E., Goede A. P. H., Visser H. and Fricke, W.: SCIAMACHY - Scanning Imaging Absorption Spectrometer for Atmospheric Chartography, *Acta Astronautica*, 35, 445-461, https://doi.org/10.1016/0094-5765(94)00278-T, 1995.

Burrows, J. P., Weber, M., Buchwitz, M., Rozanov, V., Ladstätter-Weißenmayer, A., Richter, A., DeBeek, R., Hoogen, R., Bramstedt, K., Eichmann, K.-U., Elsinger, M., and Perner, D.: The Global Ozone Monitoring Experiment (GOME): Mission Concept and First Scientific Results, *J. Atmos. Sci.*, 56, 151-175, https://doi.org/10.1175/1520-0469(1999)056<0151:TGOMEG>2.0CO;2, 1999.

Burrows, J. P., Bovensmann, H., Bergametti, G., Flaud, J. M., Orphal, J., Noël, S., Monks, P. S., Corlett, G. K., Goede, A. P. H., von Clarmann, T., Steck, T., Fischer, H., and Friedl-Vallon, F.: The geostationary tropospheric pollution explorer (GeoTROPE) missions: objects, requirements and mission concept, *Advances in Space Research*, 34, 682-687, https://doi.org/10.1016/j.asr.2003.08.067, 2004.

Callies, J., Corpaccioli, E., Eisinger, M., Hahne, A., and Lefebvre, A.: GOME-2-Metop's second-generation sensor for operational ozone monitoring, ESA Bulletin, 102, 28–36, 2000.

Edwards, D. P., Martínez-Alonso, S., Jo, D.-S., Ortega, I., Emmons, L. K., Orlando, J. J., Worden, H. M., Kim, J., Lee, H., Park, J., and Hong, H.: Quantifying the diurnal variation of atmospheric NO_2 from observations of the Geostationary Environment Monitoring Spectrometer (GEMS), *Atmos. Chem. Phys.*, 24, 8943-8961, https://doi.org/10.5194/acp-24-8943-2024, 2024.

Granier, C., Bessagnet, B., Bond, T., D'Angiola, A., van der Gon, H. D., Frost, G. J., Heil, A., Kaiser, J. W., Kinne, S., Klimont, Z., Kloster, S., Lamarque, J.-F., Liousse, C., Masui, T., Meleux, F., Mieville, A., Ohara, T., Raut, J.-C., Riahi, K., Schultz, M. G., Smith, S. J., Thompson, A., van Aardenne, J., van der Warf, G. R., and van Vuuren, D. P.: Evolution of anthropogenic and biomass burning emissions of air pollutants at global and regional scales during the 1980 – 2010 period, *Climatic Change*, 109, 163, https://doi.org/10.1007/s10584-011-0154-1, 2011.

Grell, G. A., Peckham, S. E., Schmitz, R., McKeen, S. A., Frost, G., Shamarock, W. C., and Eder, B.: Fully coupled "online" chemistry within the WRF model, *Atmos. Environ.*, 39, 6957-6975, https://doi.org/10.1016/j.atmosenv.2005.04.027, 2005.

Hong, H., Lee, H., Kim, J., Jeong, U., Ryu, J., Lee, D. S.: Investigation of Simultaneous Effects of Aerosol Properties and Aerosol Peak Height on the Air Mass Factors for Space-Borne NO_2 Retrievals, *remote sens.*, 9(3), 208, https://doi.org/10.3390/rs9030208, 2017.

Huijnen, V., Williams, J., van Weele, M., van Noije, T., Krol, M., Dentener, F., Segers, A., Houweling, S., Peters, W., de Laat, J., Boersma, F., Bergamaschi, P., van Velthoven, P., Le Sager, P., Eskes, H., Alkemade, F., Scheele, R., Nédélec, P., and Pätz, H.-W.: The global chemistry transport model TM5: description and evaluation of the tropospheric chemistry version 3.0, *Geosci. Model Dev.*, 3, 445-473, https://doi.org/10.5194/gmd-3-445-2010, 2010.

Jang, Y., Lee. Y., Kim, J., Kim, Y., and Woo, J.-H.: Improvement China point source for improving bottom-up emission inventory, *Asia-Pac. J. Atmos. Sci.*, 56, 107-118, https://doi.org/10.1007/s13143-019-00115-y, 2020.

Kim, J., Jeong, U., Ahn, M.-H., Kim, J. H., Park, R. J., Lee, H., Song, C. H., Choi, Y.-S., Lee, K.-J., Yoo, J.-M., Jeong, M.-J., Park, S. K., Lee, K.-M., Song, C.-K., Kim, S.-W., Kim, Y. J., Kim, S.-W., Kim, M., Go, S., Liu, X., Chance, K., Miller, C. C., Al-Saadi, J., Veihelmann, B., Bhartia, P. K., Torres, O., González Abad, G., Haffner, D. P., Ko, D. H., Lee, S. H., Woo, J.-H., Chong, H., Park, S. S., Nicks, D., Choi, W. J., Moon, K.-J., Cho, A., Yoon, J., Kim, S.-K., Hong, H., Lee, K., Lee, H., Lee, S., Choi, M., Veekfind, P., Levelt, P. F., Edwards, D. P., Kang, M., Eo, M., Bak, J., Baek, K., Kwon, H.-A., Yang, J., Park, J., Han, K. M., Kim, B.-R., Shin, H.-W., Choi, H., Lee, E., Chong, J., Cha, Y., Koo, J.-H., Irie, H., Hayashida, S., Kasai, Y., Kanaya, Y., Liu, C., Lin, J., Crawford, J. H., Carmichael, G. R., Newchurch, M. J., Lefer, B. L., Herman, J. R., Swap, R. J., Lau, A. K. H., Kurosu, T. P., Jaross, G., Ahlers, B., Dobber, M., McElroy, C. T., and Choi, Y.: New Era of Air Quality Monitoring from Space: Geostationary Environment Monitoring Spectrometer (GEMS), *Bull. Amer. Meteor. Soc.*, 101, E1-E22, https://doi.org/10.1175/BAMS-D-18-0013.1, 2020.

Kim, K.-M., Kim, S.-W., Seo, S., Blake, D. R., Cho, S., Crawford, J. H., Emmons, L. K., Fried, A., Herman, J. R., Hong, J., Jung, J., Pfister, G. G., Weinheimer, A. J., Woo, J.-H., and Zhang, Q.: Sensitivity of the WRF-Chem v4.4 simulations of ozone and formaldehyde and their precursors to multiple bottom-up emission inventories over East Asia during the KORUS-AQ 2016 field campaign, *Geosci. Model Dev.*, 17, 1931-1955, https://doi.org/10.5194/gmd-17-1931-2024, 2024.

Kim, S.-W., McDonald, B. C., Brown, S. S., Dube, B., Ferrare, R. A., Frost, G. J., Harley, R. A., Holloway, J. S., Lee, H.-J., McKeen, S. A., Neuman, J. A., Nowak, J. B., Oetjen, H., Ortega, I., Pollack, I. B., Roberts, J. M., Ryerson, T. B., Scarino, A. J., Senff, C. J., Thalman, R., Trainer, M., Volkamer, R., Wagner, N., Washenfelder, R. A., Waxman, E., and Young, C. J.: Modeling the weekly cycle of NO_x and CO emissions and their impacts on O_3 in the Los Angeles-South Coast Air Basin during the CalNex 2010 field campaign, *J. Geophys. Res. Atmos.*, 121, 1340-1360, https://doi.org/10.1002/2015JD024292, 2016.

Lange, K., Richter, Bösch, T., Zilker, B., Latsch, M., Behrens, L. K., Okafor, C. M., Bösch, H., Burrows, J. P., Merlaud, A., Pinardi, G., Fayt, C., Friedrich, M. M., Dimitropoulou, E., Van Roozendael, M., Ziegler, S., Ripperger-Lukosiunaite, S., Kuhn, L., Lauster, B., Wagner, T., Hong, H., Kim, D., Chang, L.-S., Bae, K., Song, C.-K., and Lee, H.: Validation of GEMS tropospheric NO_2 columns and their diurnal variation with ground-based DOAS measurements, *EGUsphere [preprint]*, https://doi.org/10.5194/egusphere-2024-617, 2024.

Levelt, P. F., van den Oord, G. H. J., Dobber, M., R., Mälkki, A., Visser, H., de Vries, J., Stammes, P., Lundell, J. O. V., and Saari, H.: The Ozone Monitoring Instrument, *IEEE Trans. Geosci. Remote Sens.*, 44(5), 1093-1101, https://doi.org/10.1109/TGRS.2006.872333, 2006.

Liu, S., Valks, P. Pinardi, G., Xu, J., Argyrouli, A., Lutz, R., Tilstra, G., Huijnen, V., Hendric, F., and Van Roozendael, M.: An improved air mass factor calculation for nitrogen dioxide measurements from the Global Ozone Monitoring Experiment-2 (GOME-2), *Atmos. Meas. Tech.*, 13, 755-787, https://doi.org/10.5194/amt-13-755-2020, 2020.

Lorente, A., Boersma, K. F., Yu, H., Dörner, S., Hilboll, A., Richter, A., Liu, M., Lamsal, L. N., Barkley, M., De Smedt, I., Van Roozendael, M., Wang, Y., Wagner, T., Beirle, S., Lin, J.-T., Krotkov, N., Stammes, P., Wang, P., Eskes, H. J., and Krol, M.: Structural uncertainty in air mass factor calculation for NO_2 and HCHO satellite retrievals, *Atmos. Mech. Tech.*, 10, 759-782, https://doi.org/10.5194/amt-10-759-2017, 2017.

Milford, J. B., Russell, A. G., and McRae, G. J.: A new approach to photochemical pollution control: implications of spatial patterns in pollutant responses in nitrogen oxides and reactive organic gas emissions, *Environ. Sci. Technol.*, 23, 1290-1301, https://doi.org/10.1021/es00068a017, 1989.

Munro, R., Lang, R., Klaes, D., Poli, G., Retscher, C., Lindstrot, R., Huckle, R., Lacan, A., Grzegorski, M., Holdak, A., Kokhanovsky, A., Livschitz, J., and Eisinger, M.: The GOME-2 instrument on the Metop series of satellites: instrument design, calibration, and level 1 data processing – an overview, *Atmos. Meas. Tech.*, 9, 1279–1301, https://doi.org/10.5194/amt-9-1279-2016, 2016.

Palmer, P. I., Jacob, D. J., Chance, K., Martin, R. V., Spurr, R. J. D., Kurosu, T. P., Bey, I., Yantosca, R., Fiore, A., and Li, Q.: Air mass factor formulation for spectroscopic measurements from satellites: Application to formaldehyde retrievals from the Global Ozone Monitoring Experiment, *J. Geophys. Res.*, 106, 14539-14550, https://doi.org/10.1029/2000JD900772., 2001.

Richter, A. and Burrows, J. P.: Tropospheric NO_2 from GOME Measurements, *Advances in Space Research*, 29, 1673-1683, https://doi.org/10.1016/S0273-1177(02)00100-X, 2002.

Rozanov, V. V., Rozanov, A. V., Kokhanovsky, A. A. and Burrows, J. P.: Radiative transfer through terrestrial atmosphere and ocean: Software package SCIATRAN, *J. Quant. Spectrosc. Radiat. Transf.*, 133, 13–71, https://doi.org/10.1016/j.jqsrt.2013.07.004, 2014.

Skamarock, W. C., Klemp, J. B., Dudhia, J., Gill, D. O., Liu, Z., Berner, J., Wang, W., Powers, J. G., Duda, M. G., Barker, D. M., Huang, X.-Y.: A Description of the Advanced Research WRF Model Version 4 (No. NCAR/TN-556+STR), https://doi.org/10.5065/1dfh-6p97, 2021.

Tilstra, L. G., de Graaf, M., Trees, V. J. H., Litvinov, P., Dubovik, O., and Stammes, P.:

A directional surface reflectance climatology determined from TROPOMI observations, *Atmos. Meas. Tech.*, 17, 2235-2256, https://doi.org/10.5194/amt-17-2235-2024, 2024.

Veefkind, J. P., Aben, I., McMullan, K. Förster, H., de Vries, J., Otter, G., Claas, J., Eskes, H. J., de Haan, J. F., Kleipool, Q., van Weele, M., Hasekamp, O., Hoogeveen, R., Landgraf, J., Snel, R., Tol, P., Ingmann, P., Voors, R., Kruizinga, B., Vink, R., Visser, H., and Levelt, P. F.: TROPOMI on the ESA Sentinel-5 Precursor: A GMES mission for global observations of the atmospheric composition for climate, air quality and ozone layer applications, *Remote Sens. Environ.*, 120, 70-83, https://doi.org/10.1016/j.rse.2011.09.027, 2012.

Williams, J. E., Boersma, K. F., Le Sager, P., and Verstraeten, W. W.: The high-resolution version of TM5-MP for optimized satellite retrievals: description and validation, *Geosci. Model Dev.*, 10, 721–750, https://doi.org/10.5194/gmd-10-721-2017, 2017.

Woo, J.-H., Choi, K.-C., Kim, H. K., Baek, B. H., Jang, M., Eum, J.-H., Song, C. H., Ma, Y.-I., Sunwoo, Y., Chang, L.-S., and Yoo, S. H.: Development of an anthropogenic emissions processing system for Asia using SMOKE, *Atmos. Environ.*, 58, 5-13, https://doi.org/10.1016/j.atmosenv.2011.10.042, 2012.

wrf-model: WRF, Github [code], https://github.com/wrf-model/WRF/release/tag/v4.4, last access: 18 May 2022.

Yang, L. H., Jacob, D. J., Dang, R., Oak, Y. J., Lin, H., Kim, J., Zhai, S., Colombi, N. K., Pendergrass, D. C., Beaudry, E., Shah, V., Feng, X., Yantosca, R. M., Chong, H., Park, J., Lee, H., Lee, W.-J., Kim, S., Kim, E., Travis, K. R., Crawford, J. H., Liao, H., Interpreting GEMS geostationary satellite observations of the diurnal variation of nitrogen dioxide (NO_2) over East Asia, *Atmos. Chem. Phys.*, https://doi.org/10.5194/acp-24-7027-2024, 2024.

List of Tables

List of Figures

Figure 8. Diurnal patterns of boundary layer mean OH concentrations over the SMA region in January (black), April (yellow), July (red), and October (blue) 2021 from the CTRL run.

Figure 9. Spatial distributions of retrieved NO_2 TropVCDs in January, April, July, and October 2021 taking the a priori data for the AMF form the TM5 run. The scenes with wind speed faster than 3m/s are excluded to minimize the impact of rapid transport.

Figure 10. Same as Figure 9, except that *a priori* values for the AMF calculation are taken from the CTRL run.

Figure 11. Similar to Figure 9, but for the differences of NO_2 TropVCD between CTRL and TM5 run (CTRL – TM5).

Figure 12. Diurnal patterns of retrieved NO_2 TropVCDs from the CTRL run in (a) January, (b) April, (c) July, and (d) October 2021 over the SMA region. Black lines indicate the NO2 TropVCD values with wind-filtered data; only the scenes with wind speed lower than 3m/s are utilized. Blue lines are the averaged values without any wind filters. The green line is for case of strong-wind run with the NO_2 TropVCD being selected and averaged for wind speeds faster than 5m/s in January.

Table 1. Description of the experimental designs. MACCity provides hourly-constant emissions, while the others provide hourly-varying emissions.

<table>
<tr><th>Run name</th><th>Model</th><th>Horizontal resolution</th><th>Emission inventory</th></tr>
<tr><td>TM5</td><td>TM5</td><td>1° × 1°</td><td>MACCity</td></tr>
<tr><td>CTRL</td><td rowspan="4">WRF-Chem v4.4</td><td>28 × 28 km^2</td><td>2021AQNEA</td></tr>
<tr><td>CONST[a)]</td><td>28 × 28 km^2</td><td>2021AQNEA</td></tr>
<tr><td>FINE</td><td>12 × 12 km^2</td><td>2021AQNEA</td></tr>
<tr><td>MIXED</td><td>28 × 28 km^2</td><td>(VOC) KORUSv5
(others) 2021AQNEA</td></tr>
</table>

[a)] CONST run uses hourly-varying emission inventory, but only data of 13:45 LT were utilized to compute AMF.

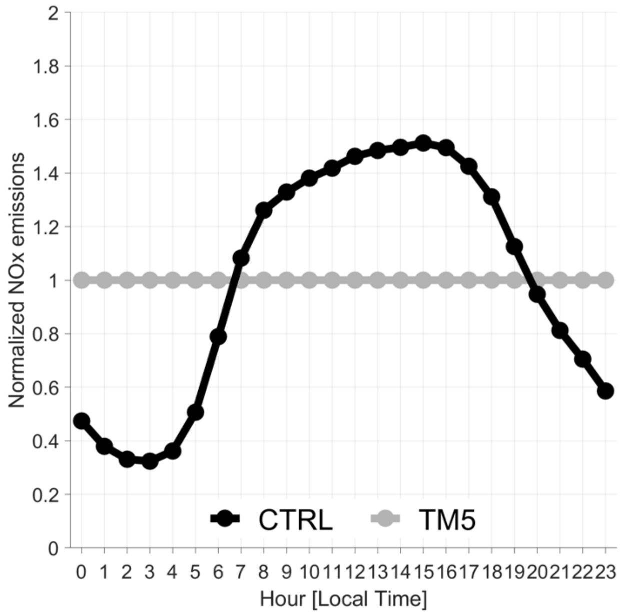

Figure 1. Diurnal variabilities of normalized NOx emissions for CTRL (black) and TM5 (gray) runs over the SMA region.

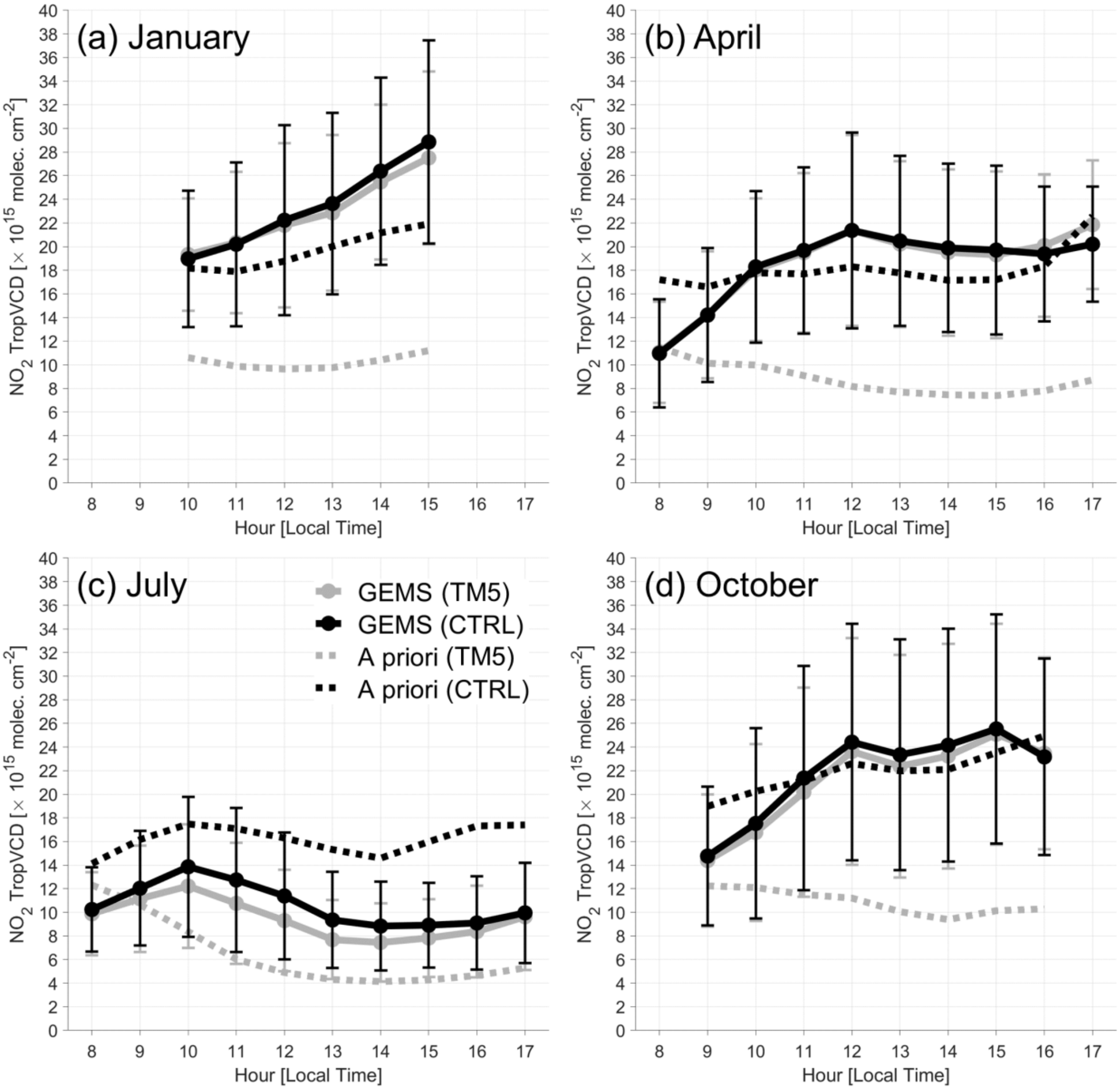

Figure 2. Diurnal behavior of retrieved (solid) and *a priori* (dashed) NO_2 TropVCDs during weekdays in (a) January, (b) April, (c) July, and (d) October 2021 over the SMA region. Gray lines identify the TM5 run, while black lines represent the CTRL run. The pixels with wind speed faster than 3m/s are excluded.

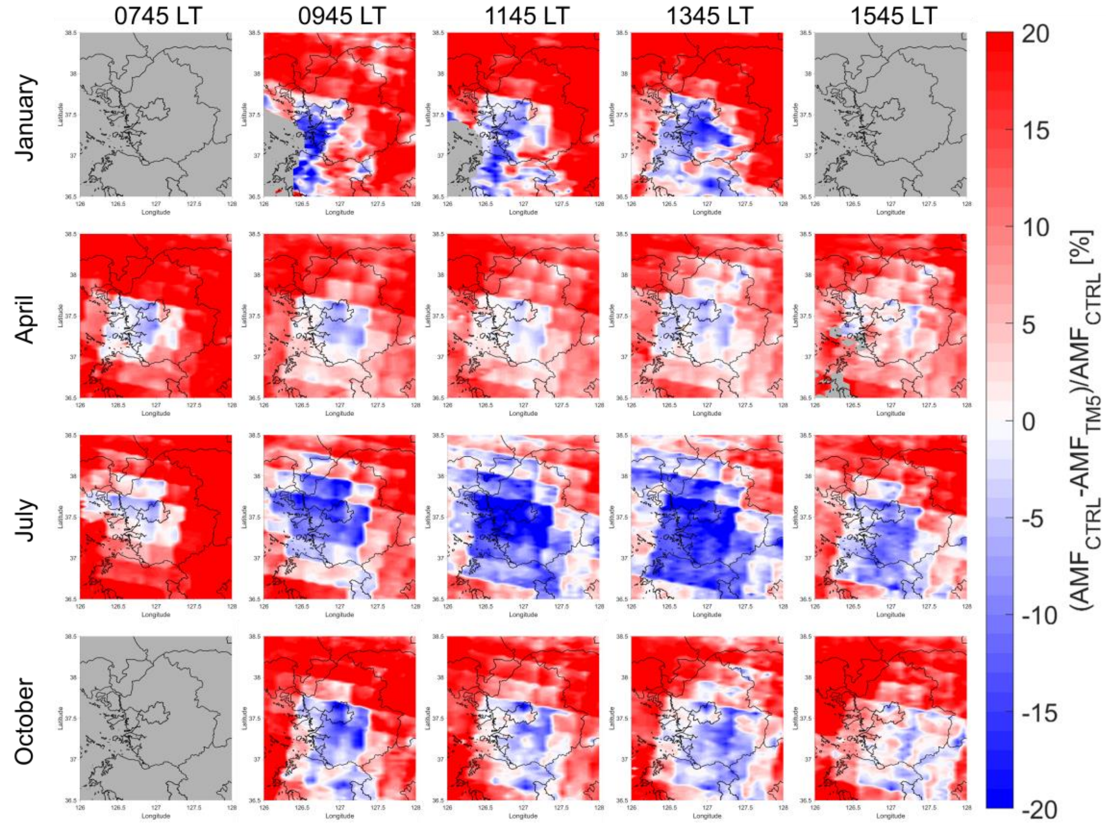

Figure 3. Spatial distributions of air mass factor (AMF) differences (CTRL – TM5) in January, April, July, and October 2021. The pixels with wind speed faster than 3m/s are excluded.

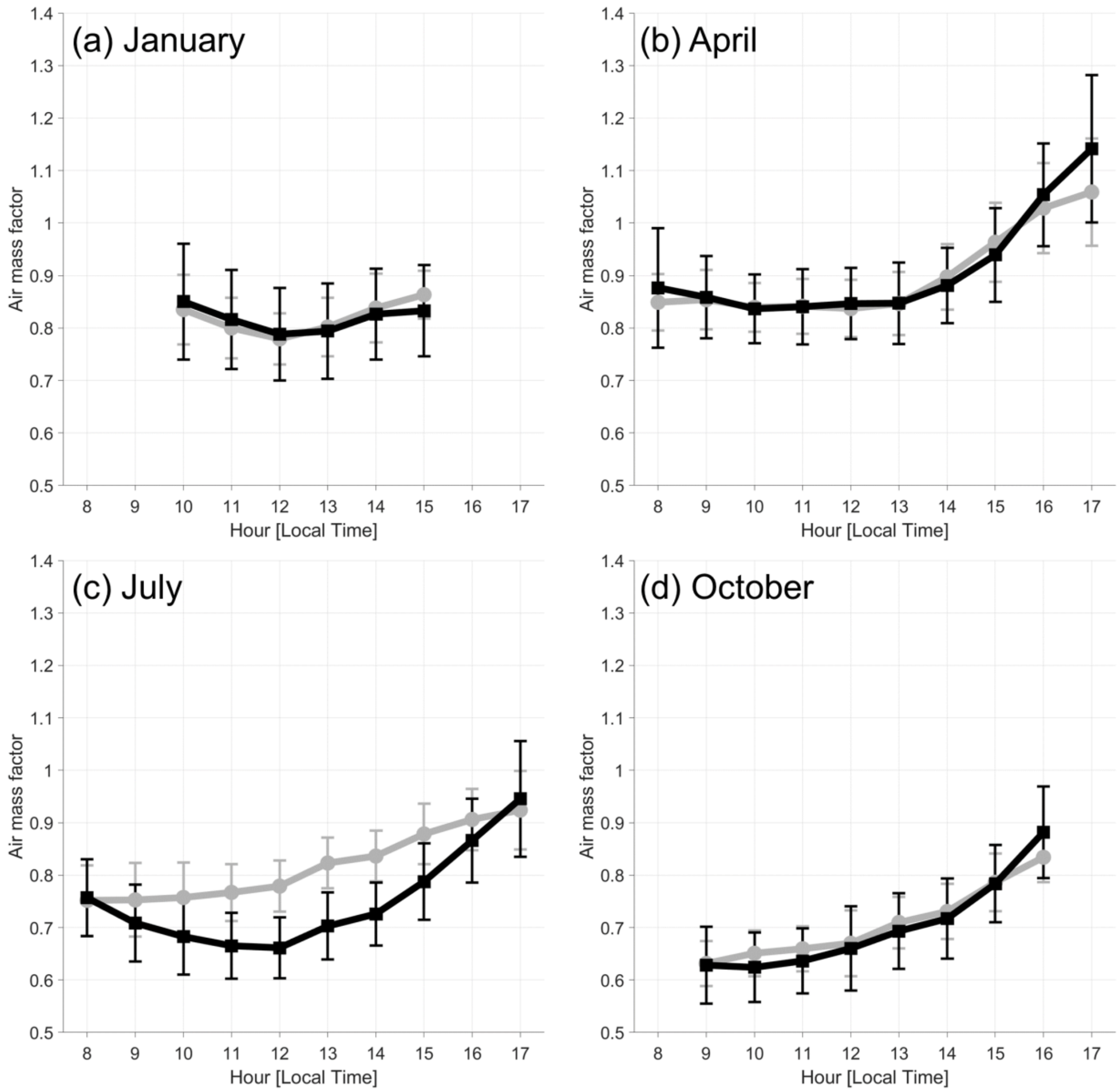

Figure 4. Diurnal patterns of the air mass factor during weekdays in (a) January, (b) April, (c) July, and (d) October 2021 over the SMA region. Gray lines indicate the TM5 run, while black lines mean the CTRL run. The pixels with wind speed faster than 3m/s are excluded.

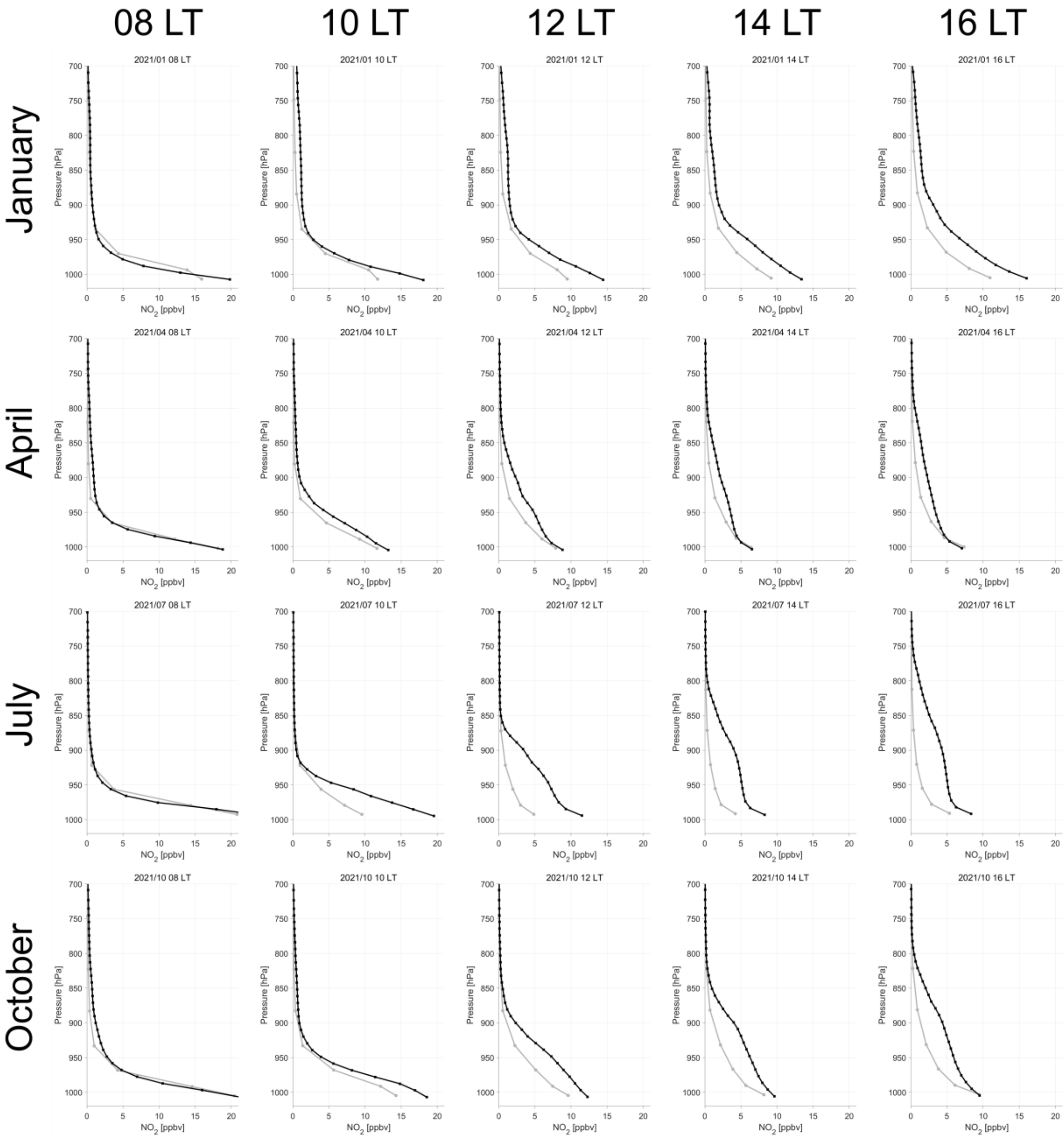

Figure 5. Vertical profiles of *a priori* NO_2 mixing ratios at 08, 10, 12, 14, and 16 LT from the TM5 (gray) and CTRL (black) runs in January, April, July, and October 2021 over the SMA region.

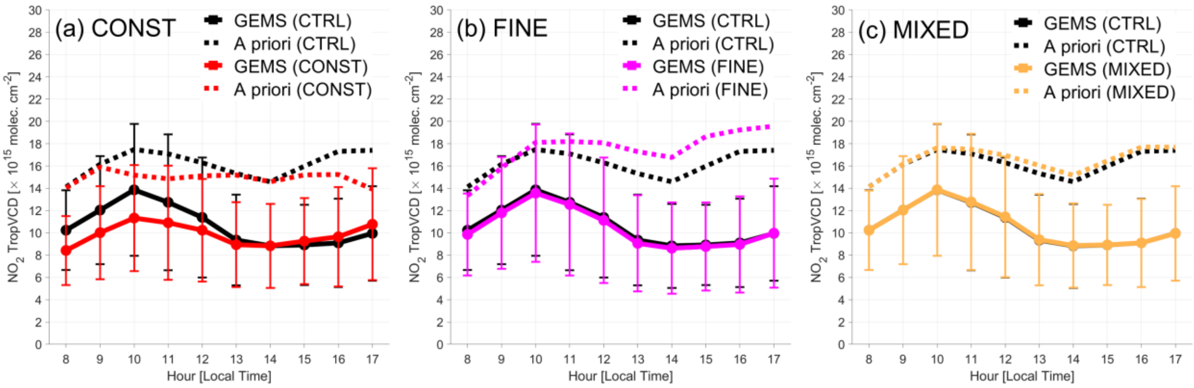

Figure 6. Diurnal patterns of retrieved (solid) and *a priori* (dashed) NO_2 TropVCDs in July 2021 over SMA region from the CTRL run (black) and (a) CONST run (red), (b) FINE run (pink), and (c) MIXED run (yellow). The pixels with wind speed faster than 3m/s are excluded. Note that diurnal changes of *a priori* NO_2 TropVCDs in the CONST run occur during calculating domain-averaged values – the location and number of pixels excluded during the collocation with satellite data vary over time during the day.

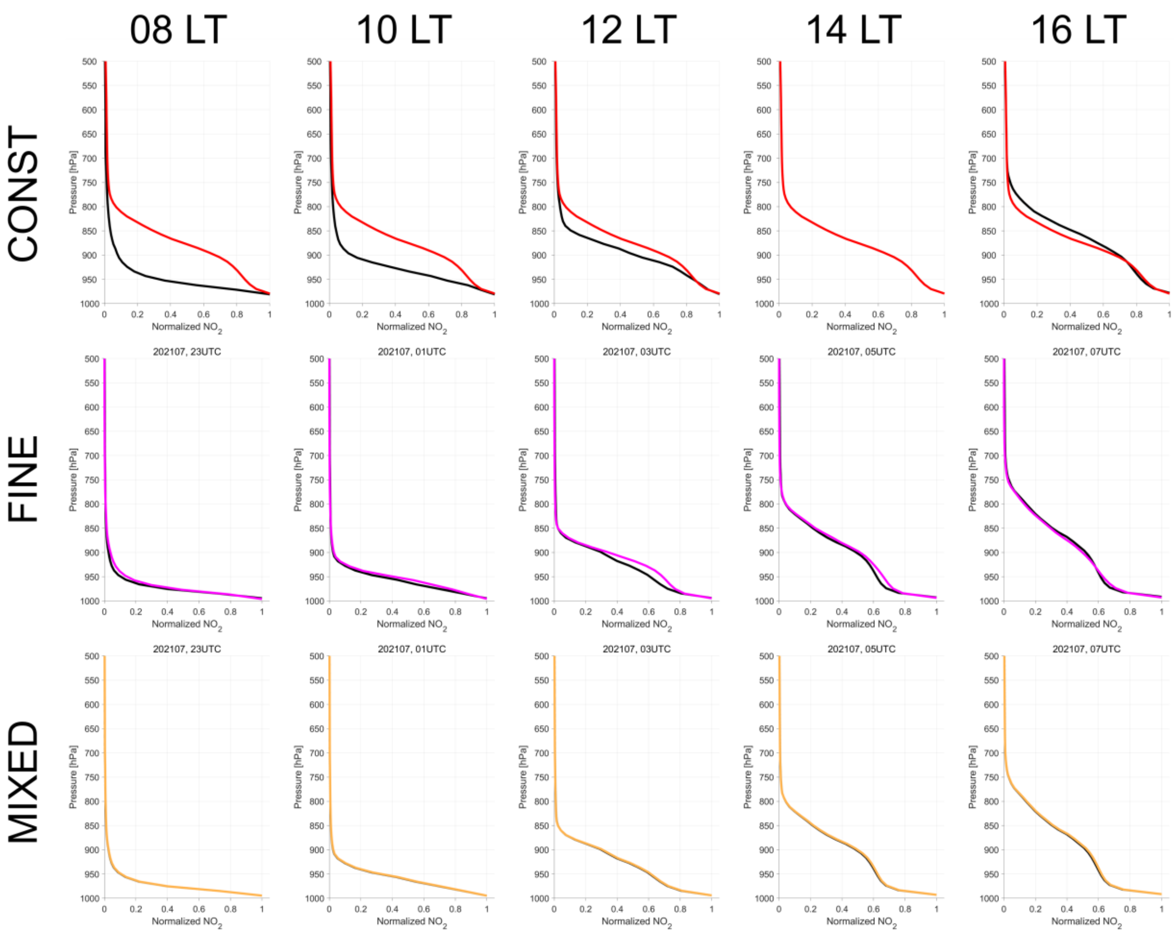

Figure 7. Vertical profiles of *a priori* NO_2 mixing ratios at 08, 10, 12, 14, and 16 LT from the CTRL (black), CONST (red), FINE (pink), and MIXED run (yellow) in January, April, July, and October 2021 over the SMA region.

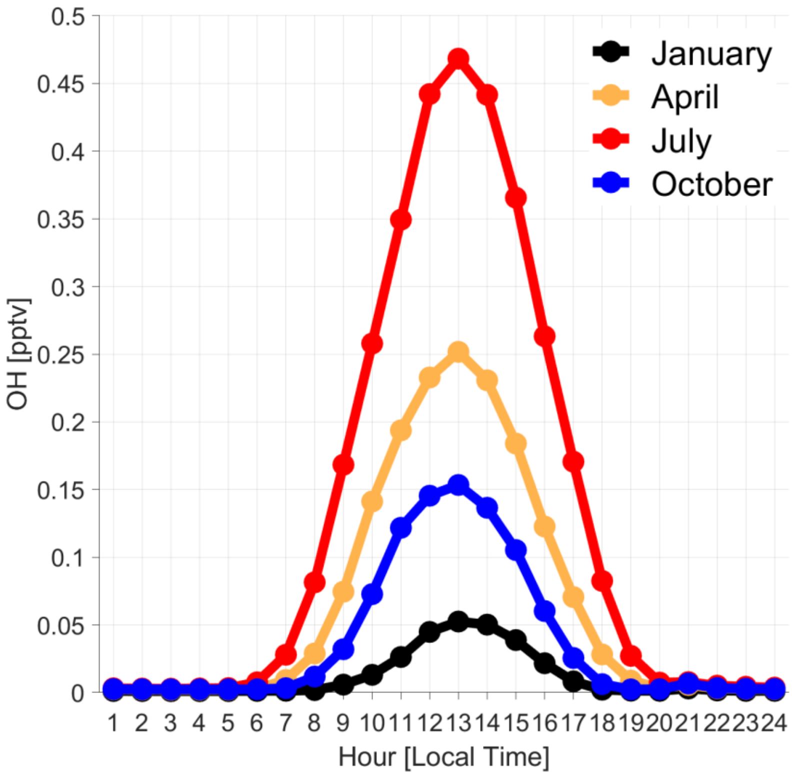

Figure 8. Diurnal patterns of boundary layer mean OH concentrations over the SMA region in January (black), April (yellow), July (red), and October (blue) 2021 from the CTRL run.

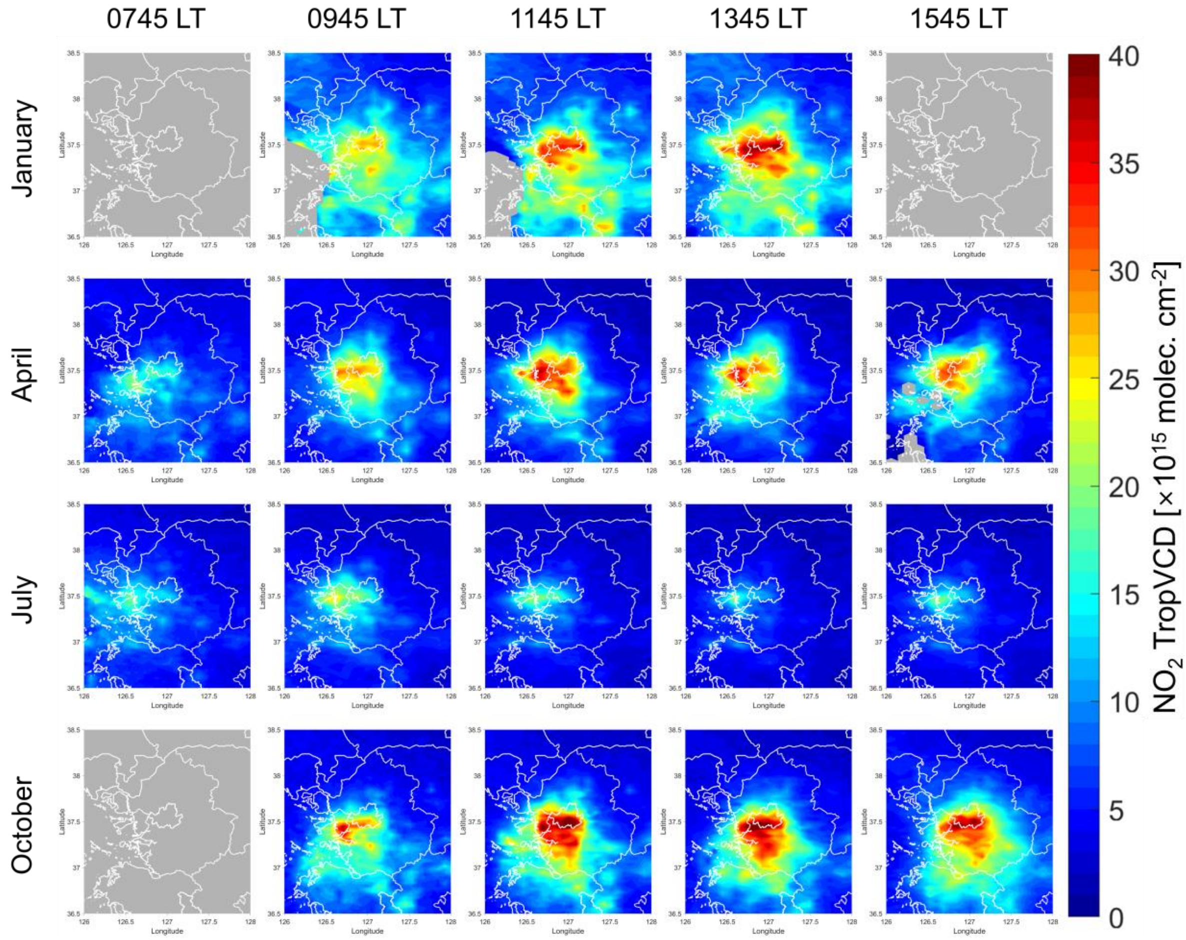

Figure 9. Spatial distributions of retrieved NO_2 TropVCDs in January, April, July, and October 2021 taking the a priori data for the AMF form the TM5 run. The scenes with wind speed faster than 3m/s are excluded to minimize the impact of rapid transport.

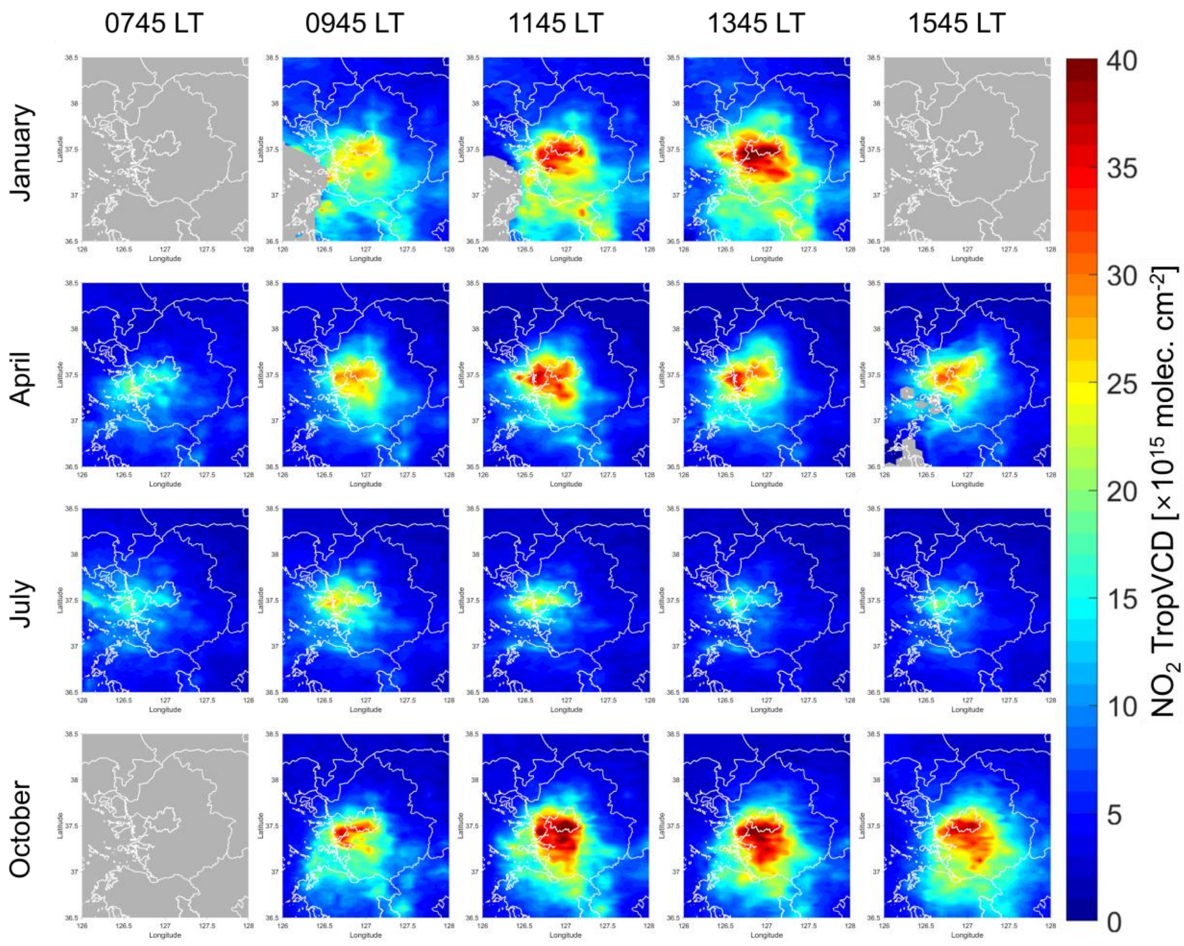

Figure 10. Same as Figure 9, except that *a priori* values for the AMF calculation are taken from the CTRL run.

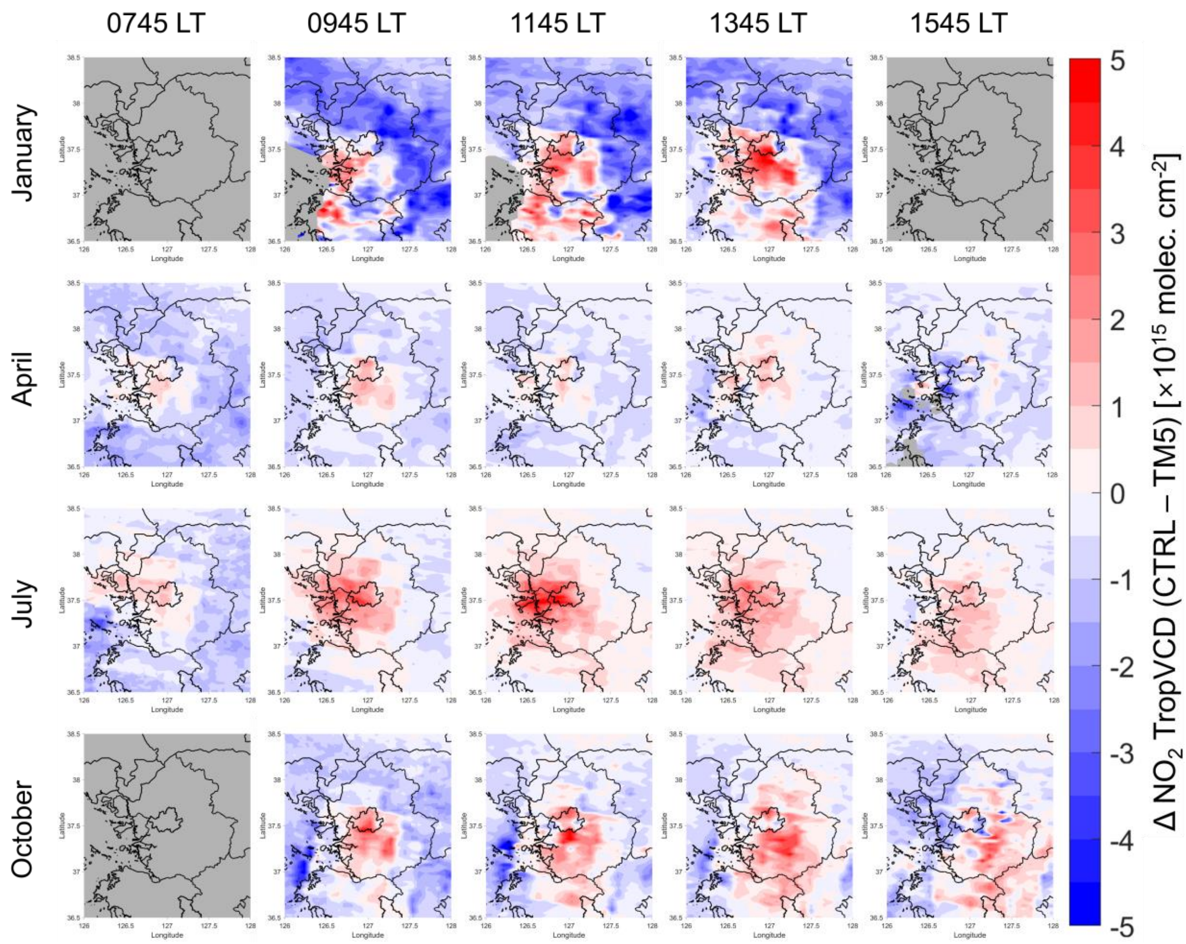

Figure 11. Similar to Figure 9, but for the differences of NO_2 TropVCD between CTRL and TM5 run (CTRL – TM5).

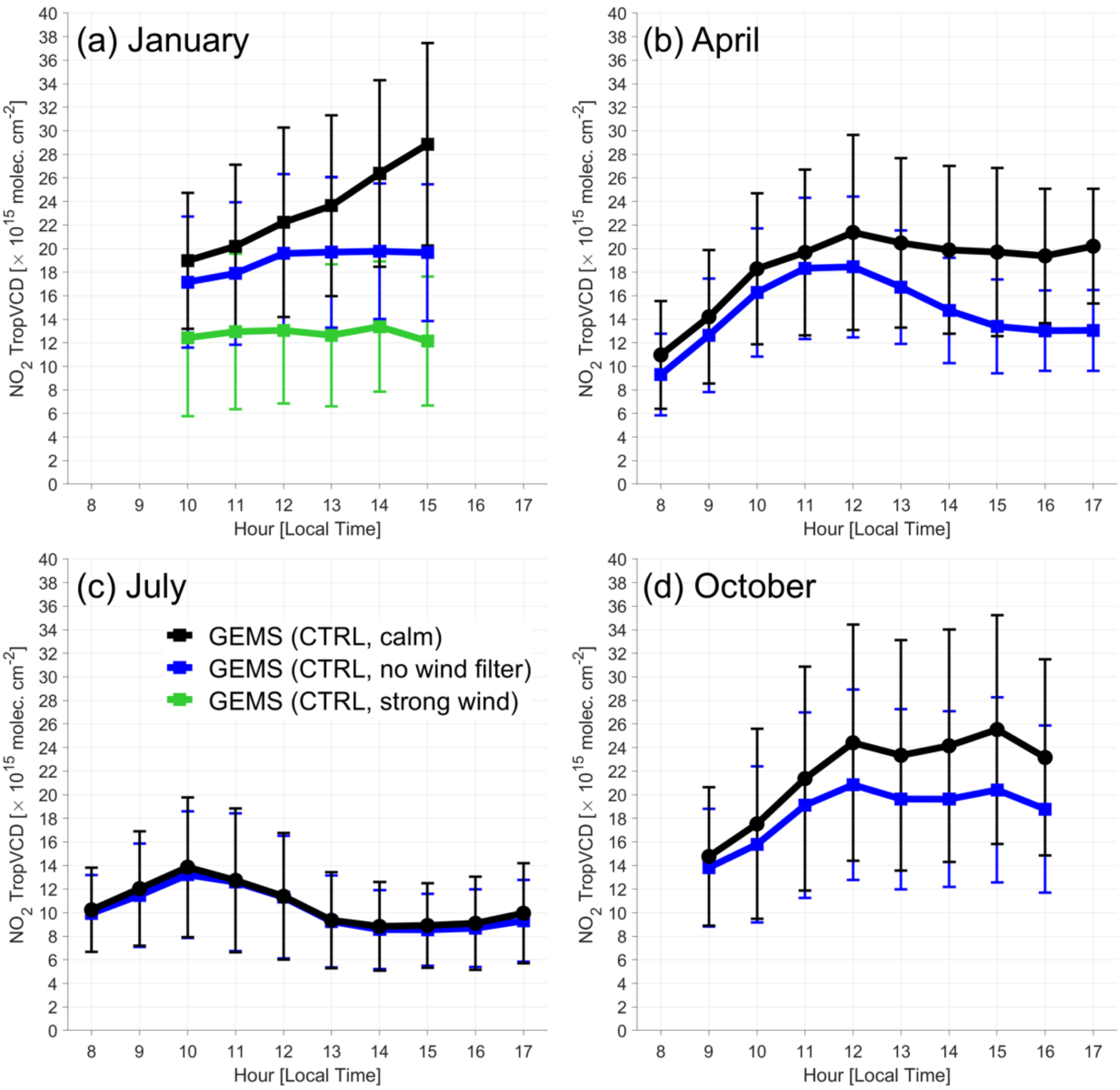

Figure 12. Diurnal patterns of retrieved NO_2 TropVCDs from the CTRL run in (a) January, (b) April, (c) July, and (d) October 2021 over the SMA region. Black lines indicate the NO_2 TropVCD values with wind-filtered data; only the scenes with wind speed lower than 3m/s are utilized. Blue lines are the averaged values without any wind filters. The green line is for case of strong-wind run with the NO_2 TropVCD being selected and averaged for wind speeds faster than 5m/s in January.